Geophysical Journal International

Geophys. J. Int. (2020) **221,** 1532–1541
Advance Access publication 2020 February 20
GJI General Geophysical Methods

doi: 10.1093/gji/ggaa087

Effects of salinity and pH on the spectral induced polarization signals of graphite particles

Yuxin Wu and Luca Peruzzo

Earth & Environmental Sciences Area, Lawrence Berkeley National Laboratory, 1 *Cyclotron Rd, MS*74-316*C, Berkeley, CA* 94720, USA.
E-mail: YWu3@lbl.gov

Accepted 2020 February 6. Received 2020 February 6; in original form 2019 June 16

SUMMARY

The electrical property of micrometre-sized graphite particles was investigated under different particle concentration, particle size, fluid conductivity and pH conditions. Due to its large internal electronic conductivity and ability to polarize under external potential field, significant enhancement of its spectral induced polarization (SIP) responses is observed when graphite is included in sand mixtures. While a small amount of graphite inclusion significantly increases the SIP response of its mixtures with sand, further concentration increase does not necessarily lead to a proportional increase of the SIP response. This is shown to be related to the formation of graphite aggregates at higher concentrations. Changes of fluid salinity have a significant effect on graphite's SIP behaviour. This includes a positive impact on normalized chargeability and imaginary conductivity, but a negative impact on chargeability and relaxation time constant. The effect of pH on the SIP response of graphite is small but shows consistent trend, where pH increase leads to a decrease of both the chargeability and relaxation time constant. The underlying cause of this effect is not clear.

Key words: Electrical properties.

INTRODUCTION

Graphite is a crystalline allotrope of carbon and an abundant Earth mineral often found in metamorphic and igneous rocks. Because of its unique thermal, electrical and mechanical properties, graphite has found many uses in a variety of industries, including electronics, refractories, steelmaking, batteries as well as in lubrication and many other applications. Constructed as many layers of 2-D sheets of honeycomb arranged carbon atoms (known as graphene), bonded by van der Waals forces, the electrical behaviour of graphite is fundamental for its many applications.

Because of its layered, planar structure, the major properties of graphite are anisotropic, which include its electrical conductivity in both single and polycrystalline forms (Krishnan & Ganguli 1939; Pedraza & Klemens 1993). The degree of anisotropy varies in natural polycrystalline graphite depending on the directionality of the arrangements of the many small crystals. While the intrinsic electrical properties of graphite have been investigated for many decades, studies on its electrical behaviour for resource exploration in the geology and environmental context have been very limited (Klein & Shuey 1978). In such systems, graphite often exists in composite with other minerals under saturated or unsaturated electrolytic conditions.

A very limited volume of research has studied the electrical behaviour of graphite in electrolytic solutions. This includes its complex conductivity or spectral induced polarization (SIP) signals (Kinchin 1953; Klein & Shuey 1978; Gurin *et al.* 2015; Revil *et al.* 2017). Early studies on the electrical properties of graphite in composites have been carried out mostly from the mineral exploration perspective. These studies compared the responses of graphite with other conducting and semi-conducting materials, such as metal sulphides, in both the linear and nonlinear impedance ranges. For instance, Klein & Shuey (1978) studied the nonlinear mineral–electrolyte interfacial impedance behaviour of graphite, together with Galena (PbS) and Chalcopyrite ($CuFeS_2$) using classic electrochemical approaches. They concluded that the nonlinear impedance at the mineral–electrolyte interface is related to the electrochemical reactions that transfer charges across the interface, that is, redox reactions, and such a behaviour is diagnostic of mineral composition. Because the energy barrier of graphite reactions is higher than those of sulphide minerals, graphite does not react when coexiting with other sulphide minerals. This suggests possible discrimination of ore types based on their impedance behaviour at the nonlinear range. Recent studies on the electrical behaviour of graphite in saturated porous media, for example, as sand mixture, have yield inconsistent results. For example, Revil *et al.* (2017) suggested that graphite, and other conductive particles, demonstrates a polarization behaviour similar to semi-conductors, such as pyrite and magnetite. The model they developed for semi-conductors suggests that the chargeability of such materials only depends on their volumetric content, independent of the pore water properties (Revil *et al.* 2015). Gurin *et al.* (2015) suggested a linear correlation

between pore water salinity and normalized chargeability, and they also suggested the impact of particle size on the chargeability (or polarization) magnitude. It is worth noting that graphite is always studied together with other minerals, and the number of data points has been very sparse. We also note the differences between the graphite particles used in these studies, for example, large cubes versus porous chunks, which may contribute to the different results and interpretations. Nevertheless, there is limited knowledge and consensus on the impacts of pore fluid chemistry, such as salinity and pH, on the electrical behaviour of graphite.

While literature disagrees on the impacts of pore fluid chemistry on the chargeability, or polarization magnitude, of conductive particles, including graphite, it tends to agree on the impact of particle size and pore water salinity on the relaxation time constant. An increasing relaxation time constant is generally associated with an increase in particle size or decrease in pore fluid salinity. This is consistent with the polarization behaviour of non-conducting materials, such as oxides and phyllosilicates, and is related to changes of the electrical double layer (EDL) properties, such as its thickness, charge density and mobility (Vinegar & Waxman 1984; Lesmes & Frye 2001; Revil & Skold 2011; Revil 2012).

CONCEPTUAL MODEL FOR CONDUCTOR POLARIZATION

Unlike non-conductive minerals with immobile internal charges, the internal charge polarization in electronically conducting materials plays the dominant role in controlling their polarization behaviours. This often results in a much large polarization magnitude with phase shift higher than 100 mrad (Slater *et al.* 2005), which is rarely observed in non-conductive minerals found in nature. As the only non-metallic electronic conductor, graphite is expected to have large polarization responses as have been observed in existing research (Klein & Shuey 1978; Gurin *et al.* 2015; Revil *et al.* 2015).

The underlying polarization process of conductors are described by a few existing conceptual models at the microscopic scale (Revil *et al.* 2015; Misra *et al.* 2016; Bucker *et al.* 2018). While these models provide valuable insights, they deviate on the key aspects of the underlying processes. These studies generally suggest an internal polarization of the metallic conductors due to the migration of negatively charged electrons and positively charged 'holes' in the opposite direction in responding to the external potential field. Such a process was suggested as 'instantaneous' by Bucker *et al.* (2018), but as 'ion-like' by Revil *et al.* (2015). In response to this internal charge polarization, ionic charges of opposite signs in the pore fluid migrate and accumulate on the opposite sides of the particles, that is, the polarization process. Because the internal charge polarization was considered instantaneous, Bucker *et al.* (2018) suggest that the relaxation time constant is controlled by the timescale of the ion migration in the pore fluids. On the contrary, the ion-like charge migration behaviour inside the conductive particles proposed by Revil *et al.* (2015) suggests a much stronger impact of the initial charge behaviour on the polarization process in terms of its magnitude and time constant.

MECHANISTIC AND EMPIRICAL MODELS

Both mechanistic and empirical models describe the SIP behaviours of electronic conductor particles with or without redox reactions. The classic Wong model describes the induced polarization behaviours of disseminated, spherical sulphide particles under the assumption of minimal interparticle interactions (Wong 1979). While such a model includes detailed formulation of the charge migration processes at mineral–electrolyte interfaces, including redox reactions, its adaptation by the community has been limited due to its complexity. The Wong model was recently re-examined and extended by Bucker *et al.* (2018). Bucker *et al.* (2018) provide a full analytical solution of the Poisson–Nernst–Planck equations to describe the polarization processes around metallic particles. They introduce a 'volume diffusion' polarization mechanism that is related to charge deficiency and surplus, due to redox reactions, that occur across mineral–fluid interfaces. Simulation results based on their model show a significant impact of redox process on the polarization behaviour of metallic particles.

Another set of mechanistic models was developed by Revil *et al.* (2015). They emphasize the charge polarization processes internal of the conductive particles due to the migration of n (−, electron) and p (+, holes) charges under the influence of an external current. To simplify the model, redox-related processes were excluded. Revil *et al.* (2015) emphasize charge mobility within the metallic particles and treat these charges as having similar polarization behaviours to ionic charges in the electrolytes. Revil *et al.* (2015) predict certain SIP behaviours that are not consistently supported by experimental results. For example, Revil *et al.* (2015) predict a simple linear relationship between the chargeability and the volume content of metallic particles, regardless of the particle sizes or pore fluid salinity. This has not consistently observed by others, for example, those presented by Gurin *et al.* (2015).

In addition to the mechanistic models described above, both semi-empirical and empirical models are used to describe the SIP behaviour of conductive particles. Such models are not aimed at describing the microscopic physicochemical processes driving the polarization response, but rather focus on deriving a set of global petrophysical parameters, such as chargeability and relaxation time constant, that relate to the characteristics of the minerals under study. Cole–Cole and Debye decomposition models are among the most frequently used (Cole & Cole 1941; Marshall & Madden 1959; Gurin *et al.* 2013; Ustra *et al.* 2016). Cole–Cole type of models are simple to use to describe SIP responses with characteristic peak frequencies and are widely used to study the SIP behaviour of metallic particles (Pelton *et al.* 1978; Slater *et al.* 2005; Revil *et al.* 2018). As empirical models, they can be widely applied to many experimental conditions that are challenging for the mechanistic models described above, for example, complex particle sizes, shapes, geometric arrangement as well as pore fluid geochemical conditions.

As discussed above, limited studies on the electrical properties of graphite have led to inconsistent conclusions regarding the effects of pore fluid chemistry, particle size and concentrations. In this study, we conducted a series of laboratory experiments with varying graphite particle sizes, concentrations, pore fluid salinity and pH with the goal to provide a systematic understanding of the SIP behaviour of graphite under these variable conditions.

MATERIALS AND METHODS

Column setup

The experiments were conducted in column apparatus constructed with schedule 40 PVC with an internal diameter (ID) of 5 cm and a length of 40 cm. Silver/silver chloride (Ag/AgCl) electrodes were

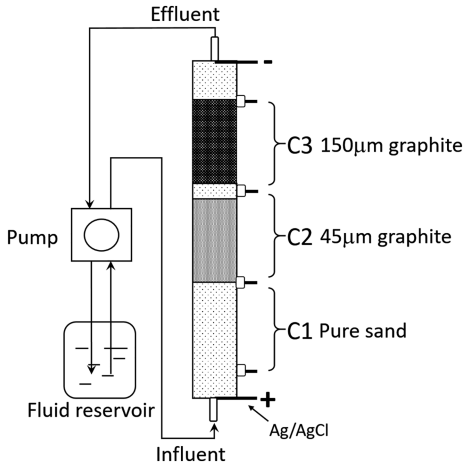

Figure 1. Schematic of the column setup for the experiments indicating the three different channels with C1: Sand only; C2: 45 μm graphite particles mixed with sand; C3: 150 μm graphite particles mixed with sand. The electrodes are made with Ag wire coated with AgCl.

installed along the length of the column for current stimulation and SIP measurements (Fig. 1). To ensure identical geochemical conditions for better comparisons between different graphite containing mixtures and baseline sand material, three separate sections of materials were consequently packed into the same column under each pore fluid treatment scenario (Fig. 1). These three different sections, called channels hereafter, were made of pure Ottawa sand (channel 1, C1), 45 μm average-sized graphite mixed with sand (channel 2, C2) and 150 μm average-sized graphite mixed with sand (channel 3, C3; Fig. 1). A 1″ sand section was packed between the two graphite channels, C2 and C3, to minimize interferences. The materials were dry packed into the column and flushed with CO_2 gas overnight to remove air before fluid saturation. The column was vertically positioned and the saturating fluids were injected from the bottom. The saturation was carried out in a looped configuration where effluent from the top of the column was returned into the influent reservoir, mixed and re-circulated back into the column. This configuration allows the establishment of a steady-state condition within the column across the different channels. The conductivity of the reservoir fluid was monitored periodically, and the measurements of the SIP responses were only carried out after stabilization of both the bulk conductivity of the column and fluid conductivity in the reservoir. This process typically took less than 24 hr under a flow rate of ∼1 pore volume per hour.

The saturating fluids used in the experiments were (1) sodium chloride (NaCl) solutions at different molar concentrations (10, 20, 40, 80 and 160 mM) under constant pH (7 ± 1) and (2) NaCl solutions with constant molar concentration (160 mM, fluid conductivity = 17 ± 0.5 mS cm^{-1}) under different pH conditions (2.73, 3.85, 5.33, 7.55, 9.26, 9.79 and 10.83). The experiments were conducted by systematically varying graphite concentration, particle size and pore fluid chemistry. As shown in Table 1, experimental sets 1–3 represent graphite concentrations at 5, 10 and 15 per cent for C2 (45 μm) and C3 (150 μm). The sand only channel (C1) serves as the baseline comparisons. Each set of the experiments went through the sequence of doubling NaCl fluid molar concentrations from 10 to 160 mM. At the end of the experiment set #1 with 5 per cent graphite, the pH experiments were conducted with pH varied from 2.73 to 10.83 as listed in Table 1.

The graphite materials used in the experiments were micrometre (μm) sized, planar graphite particles acquired from Sigma Aldrich. The materials were characterized by scanning electron microscope (SEM) and BET (Brunauer–Emmett–Teller) surface area measurements. Two example SEM images of the graphite/sand mixture (5 per cent) are shown in Fig. 2. SEM images suggest a geometric arrangement of graphite particles as a combination of surface attached smaller particles and intergrain filling of larger particles. Based on BET measurements, the specific surface area for the 45 μm graphite is 1.55 m^2 g^{-1}, and for the 150 μm graphite is 2.68 m^2 g^{-1}. The surprisingly higher specific surface area of the 150 μm graphite suggests that there might be a larger fraction of fine particles in the 150 μm graphite. This is reflected in the SIP data, which will be discussed later.

SIP data acquisition

The SIP data sets were collected with a data acquisition system based on a National Instrument signal analyser (NI 4461) in the frequency range from 0.1 to 10 K Hz. Sinusoidal waveforms were used as the excitation current source with a peak-to-peak magnitude at 2 V. This input electrical signal swipes through the frequency range at a rate of 10 measurements per decade that are evenly distributed on the logarithmic scale. The output of the data acquisition system includes a resistance magnitude and a phase shift (against the excitation signal). The accuracy of the resistance measurements is within 1 per cent, and for the phase shift measurements, within 1 milliradians (mrad) up to 1000 Hz, and 10 mrad up to 10 000 Hz based on tests conducted on the same columns filled only with electrolytes. The complex electrical, or SIP, data can be present in forms of complex resistivity ($\rho*$), conductivity ($\sigma*$) or dielectric permittivity ($\varepsilon*$). In terms of conductivity, its real (σ') and imaginary (σ'') components can be calculated based on a conductivity magnitude ($|\sigma|$) and a phase shift (ϕ) term that are outputs from the data acquisition system using the following equations:

$$\sigma' = |\sigma| \cos(\phi) \tag{1}$$

$$\sigma'' = |\sigma| \sin(\phi). \tag{2}$$

While the real component of the electrical signal measures the ability of the material to conduct (or impede) flow of electrical charges, the imaginary component is linked to the charge polarization that predominantly occurs at the mineral–electrolyte interface at low frequencies. Porosity, permeability, mineralogy, pore fluid saturation, salinity and temperature are among the factors affecting the magnitude of both the real and imaginary electrical signals. While electrical charge conduction occurs primarily through both interconnected pore spaces and the mineral surface, the low-frequency polarization signal is primarily an electrochemical phenomena occurring in the EDL at the mineral—electrolyte interface (Wong 1979; Merriam 2007; Placencia-Gómez & Slater 2014). For electronically conductive materials, such as graphite and metals, additional charge conduction and polarization at the mineral–electrolyte interface occurs via the polarization of internal charges of the conductors as discussed above.

The SIP data sets acquired from these experiments mostly exhibit classic Cole–Cole type of shape with characteristic peak polarization frequencies, and are therefore modelled empirically with the Cole–Cole model (Cole & Cole 1941). The Cole–Cole model has been used in different forms (Tarasov & Titov 2013), and one of

Table 1. A summary of the different sets of experiments under variable graphite concentration, size, pore fluid salinity and pH conditions.

Experimental Set	Channels	Matrix composition	Pore fluid tests (mM)	pH tests
1	1	Sand	10, 20, 40, 80, 160	2.73, 3.85, 5.33, 7.55, 9.26, 9.79, 10.83
	2	5% 45 μm graphite		
	3	5% 150 μm graphite		
2	1	Sand	10, 20, 40, 80, 160	Not tested with variable pH
	2	10% 45 μm graphite		
	3	10% 150 μm graphite		
3	1	Sand	10, 20, 40, 80, 160	
	2	15% 45 μm graphite		
	3	15% 150 μm graphite		

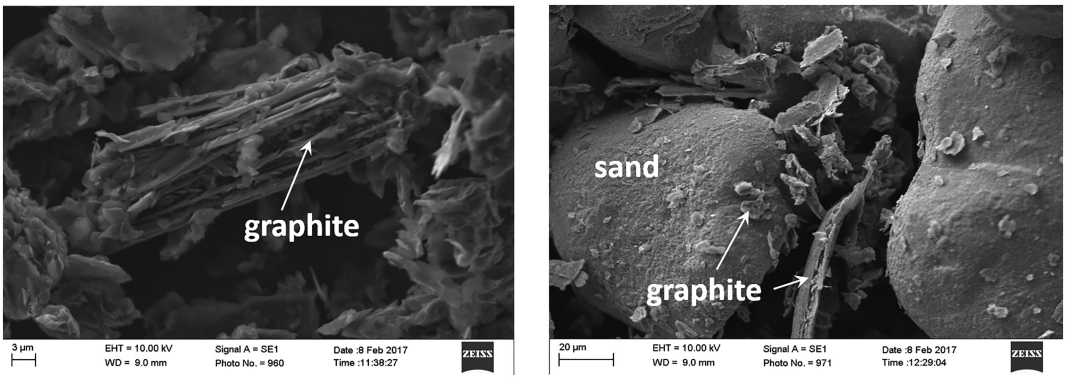

Figure 2. Example SEM images of the platelet graphite particles mixed with silica sand.

them in terms of the complex conductivity ($\sigma*$) is derived by Pelton *et al.* (1978) and is shown as

$$\sigma^* = \sigma_0 \left[1 + m \left(\frac{(i\omega\tau)^c}{1 + (i\omega\tau)^c (1 - m)} \right) \right], \quad (3)$$

where σ_0 is the conductivity at DC frequency, ω is the angular frequency, τ is the mean relaxation time, c is a shape exponent (typically 0.1–0.6) and m is the chargeability, an indicator of the polarization magnitude. When experimental results display relaxation spectrums that do not fit one-term Cole–Cole model, for example, showing double peaks, multiple Cole–Cole terms can be applied to fit the data. As will be discussed later, we used a two-term additive Cole–Cole model for some results from our experiments that displace double peak characteristics.

RESULTS

Baseline comparison with pure sand

As evident from Fig. 3, inclusion of graphite particles significantly increased the SIP signal of silica sand mixtures, particularly the phase responses. While the phase response from pure silica sand is negligible, 5 per cent graphite addition is able to increase the overall phase response at peak frequencies to ~100 mrad (Fig. 3a). Note that the phase response for the 150 μm graphite column at peak frequencies is higher than that of the 45 μm graphite. As the specific surface area is a major factor affecting phase responses, this is in agreement with the higher surface area of the 150 μm graphite measured by BET, suggesting a higher fraction of fine particles in this material. It is worth noting the higher real conductivity signal for the 45 μm graphite at low frequencies (Fig. 3b). This does not occur for the 150 μm graphite.

Graphite concentration effects

As the concentration of graphite particles increases, a drastic change of the SIP behaviours is observed. This includes a deviation between C2 and C3, the two channels with two different particle sizes (45 and 150 μm; Fig. 4). The data shown in Fig. 4 are for the experiments with 10 mM NaCl at pH 7 $\pm$ 1, but similar responses are observed under other salinity conditions. For C2 with 45 μm graphite, a significant decrease of the high-frequency (>100 Hz) phase response is observed when its concentration increases to 10 per cent. Further decrease is observed at 15 per cent (Fig. 4a). While high-frequency phase response decreases, concurrent increase at low frequency, for example, at 0.1 Hz, is evident. The lower frequency phase response seemingly peaks at frequencies < 0.1 Hz that were not captured in the frequency range applied. The real conductivity signals from 45 μm graphite showed a large increase by more than 100 per cent when graphite concentration increased from 5 per cent to 10 per cent. Further concentration increase to 15 per cent led to additional, but smaller, increase in real conductivity.

The 150 μm graphite displays a different behaviour, and the changes of both the phase and conductivity with concentration are more gradual. Specifically, a small increase of both the phase and conductivity is observed when the graphite concentration increases from 5 per cent to 10 per cent. A clear shift of the high-frequency phase peak from ~ 200 Hz to < 100 Hz is also evident. An emerging upward increase of the phase response at >1000 Hz is also observed. Further increase to 15 per cent graphite results in a general decrease of the higher frequency phase response with a concurrent increase at the lower frequency. This is similar to the observation from the 45 μm graphite measurements. Increase of graphite concentration from 10 per cent to 15 per cent brought a large increase of conductivity by > 50 per cent comparing to the previous increase from 5 per cent to 10 per cent.

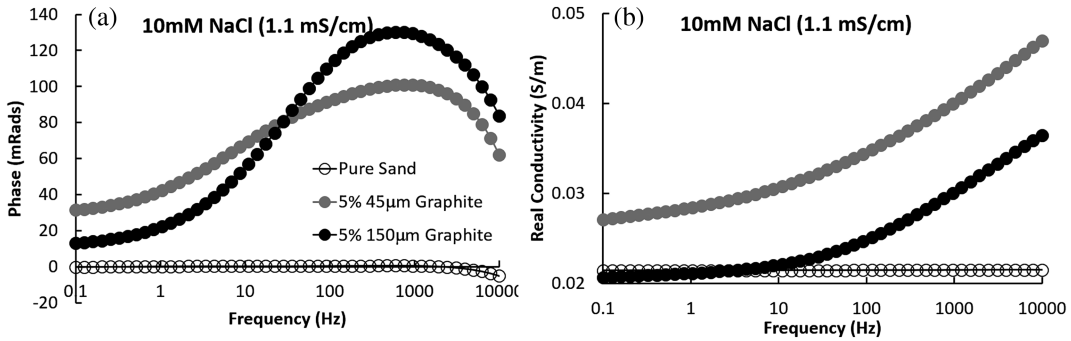

Figure 3. The effects of graphite inclusion on the SIP signals (a—phase shift; b—real conductivity) of Ottawa sand with 5 per cent of 45 and 150 μm particles. The saturating fluid is 10 mM NaCl solution at pH $\sim$ 6.8.

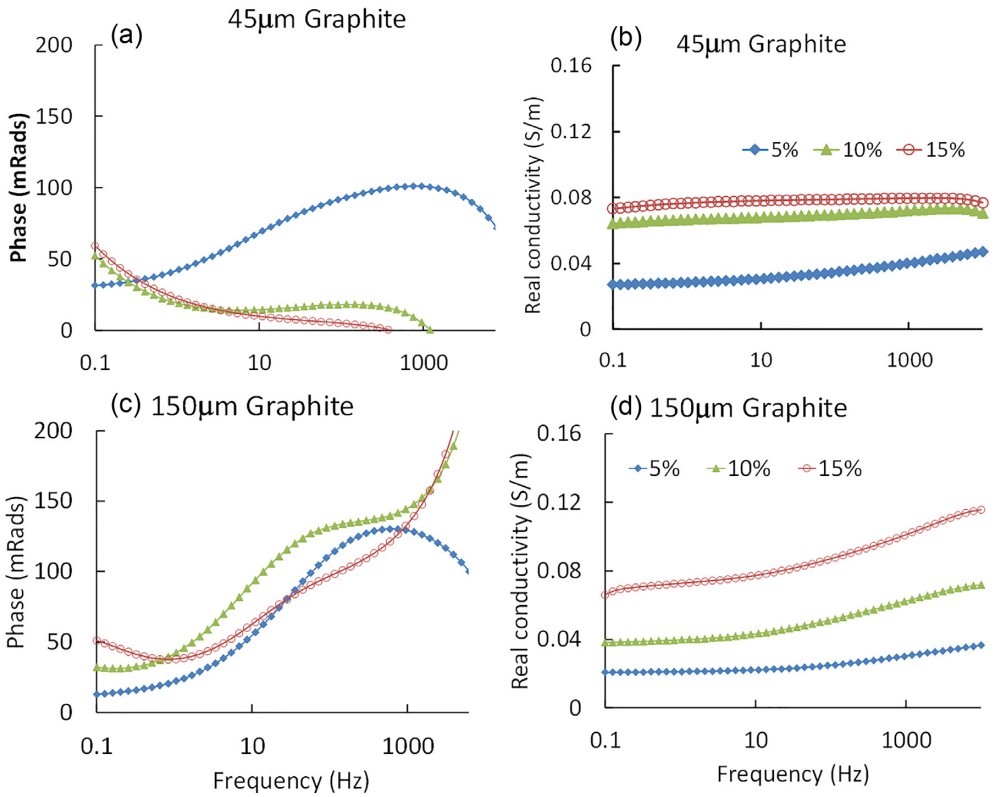

Figure 4. The effects of graphite concentration on the SIP response for both phase response (a and c) and real conductivity (b and d). Increasing concentrations with 5, 10 and 15 per cent of graphite are shown for both the phase response and real conductivity.

Fluid salinity and pH effects

The significant impact of salinity/solute concentration on the SIP responses of graphite is clearly observed in our experiment (Fig. 5). In general, increasing salinity results in a consistent shift of phase peaks to higher frequencies, yet its impact on the magnitude of the phase response is inconsistent. The 150 μm graphite data sets displayed a consistent decrease of the polarization magnitude with increasing salinity (Figs 5d–f), this is not the case in the 45 μm graphite measurements. In particular, there seems to be a mere shift of the spectrum to the higher frequency without much magnitude change for the 5 per cent case, but a decrease of the lower frequency (<1 Hz) phase magnitude and at the same time an increase of the high-frequency peak magnitude for the 10 and 15 per cent cases. As later evidence suggests, only the 5 per cent 150 μm graphite case can be treated as a well dispersed case, while other experiments have a variable degree of particle interconnection. These will be discussed in the contexts of other data sets later.

Unlike the phase response, the imaginary conductivity shows a consist increase with increasing fluid conductivity (Fig. 6). This is observed for all six different cases. However, despite the general consistency in terms of salinity effects on imaginary conductivity, there is still a different behaviour between the 45 and 150 μm graphite cases with increasing graphite concentration. In general, the magnitude of the imaginary conductivity is smaller in the 45 μm than the 150 μm graphite cases. Additionally, the 45 μm graphite cases show a relatively small change of the high-frequency response, but a significant increase of the low-frequency signals (Figs 6a–c). This is especially true at 15 per cent concentration. On the other

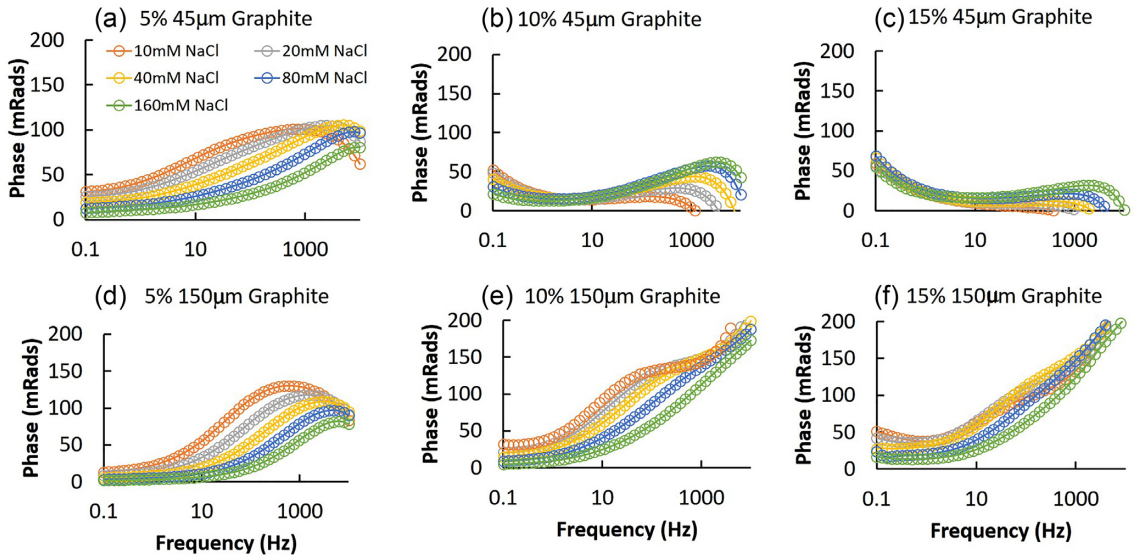

Figure 5. The effects of fluid salinity on the phase responses of graphite particles at 5, 10 and 15 per cent concentrations.

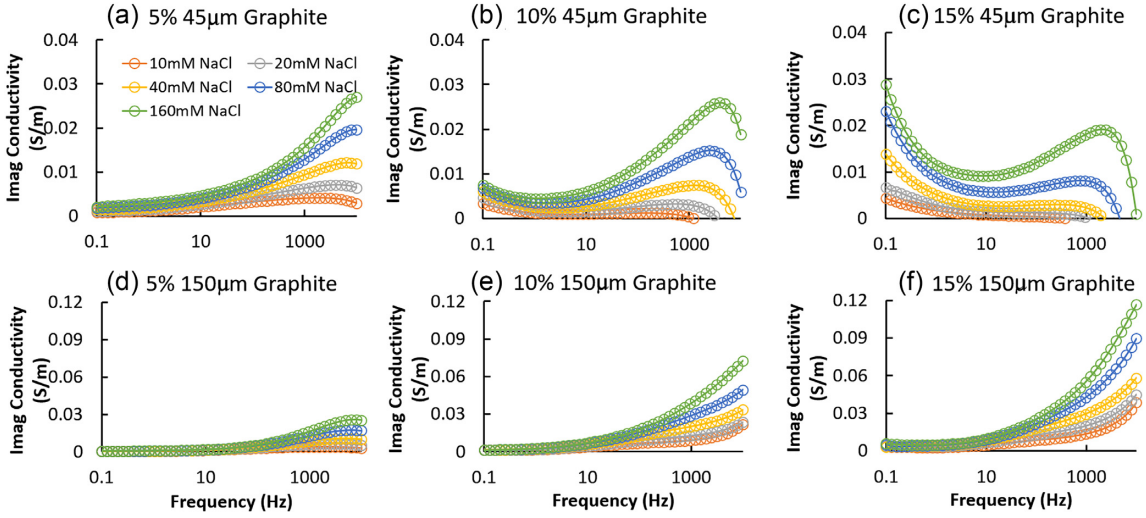

Figure 6. Changes of imaginary conductivity during the salinity tests for the different set of experiments with variable graphite concentration and size.

hand, the 150 μm graphite case showed a large increase of the high-frequency signals with increasing graphite concentration, with an observable, yet small increase, at low frequencies (Figs 7d–f).

The effects of pH on the polarization response of graphite are small, but consistent (Fig. 7). A small conductivity fluctuation (<5 per cent) is present across the different pH conditions (Figs 7b and e). However, this variation of fluid conductivity does not show a consistent pattern within pH changes. Despite the fluid conductivity fluctuation, a consistent decrease of the phase response and imaginary conductivity is observed with increasing pH (Figs 7a, c, d, f). This is also consistent for the two different sized particles tested in these experiments.

Cole–Cole model results

Fitting of the experimental data with Cole–Cole model is fairly straightforward and some examples of the model fitting results are shown in Fig. 8. Note that either one or two Cole–Cole terms are used to fit the results depending on the characteristics of the data. For instance, the data sets for 5 per cent 150 μm graphite display a singular characteristic peak and are therefore modelled with only one Cole–Cole term (Fig. 8a). On the contrary, those data sets with binary characteristic are fitted with two Cole–Cole terms as shown in Fig. 8(b) for 10 per cent 45 μm graphite measurements. Note that we did not capture the low-frequency peaks for those data sets with binary characteristics. The Cole–Cole modelling of these data sets is likely less accurate.

The effects of fluid conductivity and pH on Cole–Cole model derived polarization magnitude (m) and relaxation time constant (τ) are explored (Fig. 9). Trend lines of the data sets are shown to better illustrate the trends. It is apparent from Fig. 9 that changes of fluid conductivity have a consistent impact on both the polarization magnitude and time constant across the different graphite particle sizes and concentrations studied. Note that m represents the polarization term with peak frequencies at > 100 Hz for those data set displaying a single peak, but the lower frequency peak when

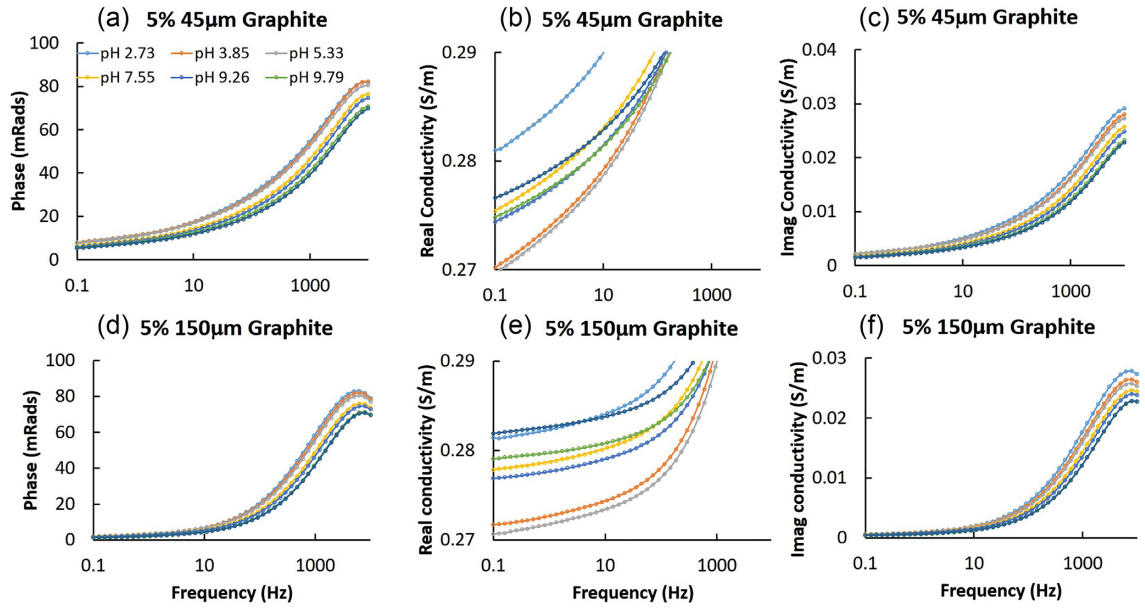

Figure 7. The effects of pH on phase response, real and imaginary conductivity for both 45 and 150 μm particle sizes at 5 per cent concentration.

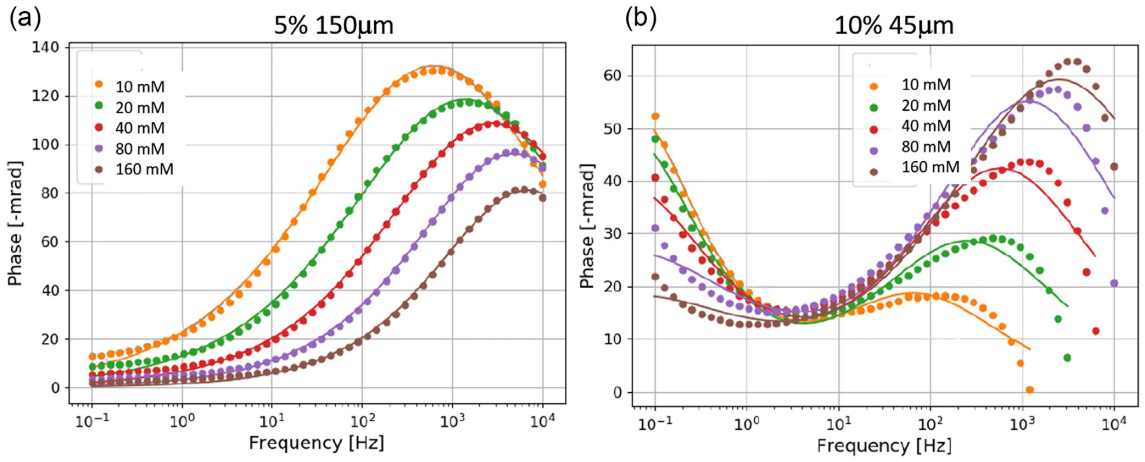

Figure 8. Examples of the Cole–Cole model fitting of the data sets. The points represent data and the lines are the modelling fits. Two additive Cole–Cole terms are used for the model simulation.

two peak frequencies co-existed. Fig. 9 shows that the lowest concentration (5 per cent) of the 150 μm graphite displays the largest polarization response at $>$ 100 Hz. Fig. 9 also shows that changes of fluid pH have a consistent impact on both the polarization magnitude and the relaxation time constant, displaying a decreasing trend with increasing pH for both particle sizes.

Literature on non-conducting oxide or phyllosilicate minerals has suggested a normalization procedure for the chargeability term, m, to eliminate the effect of changing fluid conductivity on chargeability (Slater & Lesmes 2002) to facilitate data comparison. This is typically carried out by dividing m by bulk resistivity, or multiplying by conductivity. While the underlying physics of this treatment, particularly its applicability to conductors, is not clear, we conducted such a transformation for better comparison with literature. As can be seen from Fig. 10, the normalized chargeability (m_n) displaces a reversed behaviour with changing fluid conductivity when compared with chargeability (m), that is, an increase with increasing fluid conductivity instead of decrease. Again, the 5 per cent 150 μm graphite still shows the largest values across all fluid conductivities.

DISCUSSION

Large effect of graphite on SIP

The experimental results clearly indicate the large effect of graphite inclusion on the SIP behaviour of a porous media (silica sand in this case) as shown in Fig. 2. The phase responses at peak frequency with 5 per cent graphite are close to, or higher than, 100 mrad, far exceeding those observed for zero valent iron, which is well known for its large polarization responses (Slater *et al.* 2005). Such a large response is due to the high electronic conductivity of graphite and, maybe more importantly, the lack of oxides on its surface due to its extreme stability and non-reactivity. Most metallic minerals engage in some level of redox reactions when in contact with water resulting in the formation of an oxide layer on the surface that could dampen the polarization response of the materials. This is not the case for graphite. Another reason for the high polarization magnitude in our study is related to the small sizes and the platelet shape of the graphite particles that result in a large amount of polarizable surface area.

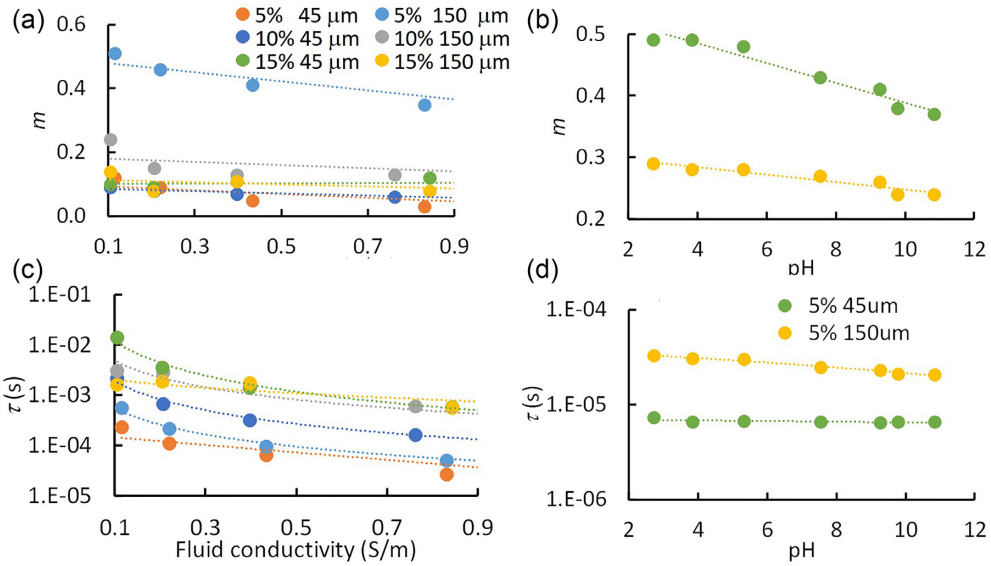

Figure 9. The effects of fluid conductivity and pH on the polarization magnitude, m, and relaxation time constant, τ, based on Cole–Cole models for the different sets of experiments. A linear trend line is shown for each data set.

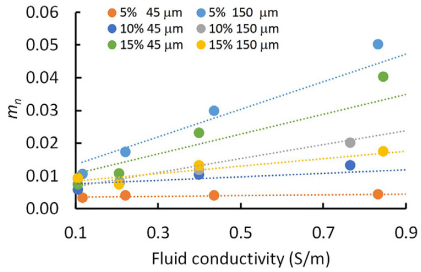

Figure 10. The effects of fluid conductivity on the normalized polarization magnitude, m_n, for the different sets of experiments. A linear trend line is shown for each data set.

Fluid conductivity and pH effects

The effects of pore fluid salinity on the polarization behaviour of graphite particles show deviations from literature. For instance, Revil *et al.* (2018) concludes that fluid conductivity, or salinity, has no effects on chargeability of conductive particles including graphite, yet our results suggest a strong effect. Specifically, an increasing fluid conductivity leads to a systematic increase of the normalized chargeability as shown in Fig. 10. However, the effect of fluid conductivity on phase response and un-normalized chargeability shows a decreasing trend in general, particularly for the well dispersed case with 5 per cent 150 μm graphite. With the normalized chargeability, our results seem to be consistent with those observed by Gurin *et al.* (2015) where they also observed an increase of normalized chargeability with increasing fluid conductivity based on synthesis of data from a variety of conducting or semi-conducting minerals.

While there is disagreement in terms of the correlations between chargeability, or normalized chargeability, and fluid salinity, the changes of imaginary conductivity and relaxation time with fluid salinity are largely consistent with previous research (Gurin *et al.* 2015). Specifically, an increasing imaginary conductivity and decreasing relaxation time constant are observed with increasing fluid salinity. The polarization of conductive particles initiates from the pore fluids and subsequently extends to the conductive particles. Therefore, the charge properties of the ions in the pore fluid, for example, charge density, mobility, are important for the electrical behaviour of the material. As a result, the magnitude, charge density, and the relaxation behaviour of charges on graphite surface are likely strongly impacted by the properties of the ions in the pore fluids. An increase in fluid salinity leads to a more compact EDL structure with a smaller Debye length, and subsequently a shift in both the polarization magnitude and relaxation time constant.

The effects of pH on both the chargeability and relaxation time constant show consistent trends with both types of particle sizes. Because the fluid conductivity is kept constant during the pH variation experiments, the possibility of fluid conductivity variation as the underlying cause of the observed polarization behaviours can be excluded. Previous experimental and modelling studies on non-conductive media, such as sandstones, suggest that pH effect on SIP is only secondary (Lesmes & Frye 2001; Skold *et al.* 2011; Peruzzo *et al.* 2018) and is primarily realized through its impact on charge density in the EDL. In the case of graphite, because there is limited understanding of the EDL properties of graphite, such an effect is difficult to evaluate. Because the electrical charge structure on graphite surface is primarily induced by external excitation, we suggest there is no preferential selection of the ion species to accumulate on the graphite surface during the polarization processes. Based on a rough calculation the Na^+: H^+ ratio, and Cl^-: OH^- ratio, is mostly > 1000:1 during the experiment. This suggests that Na^+ and Cl^- ions should have the dominant control on the polarization process, and those directly from H^+ and OH^- are negligible. However, the changes of the polarization magnitude m by ~20 per cent (Fig. 9b) with pH increase from ~ 2 to 11 suggest a larger effect disproportional to the negligible contributions of the H^+ and OH^- to the overall charged ions in the pore fluid. As a result, we postulate that the effect of changing pH on the induced polarization signature is likely through their impacts on Na^+ and Cl^- ions, such as their ionic mobility. The consistency between the two separate data set suggest the small, yet consistent, pH effect on the SIP response of graphite is likely realistic, although it underlying mechanism is not clear. Further investigation is needed.

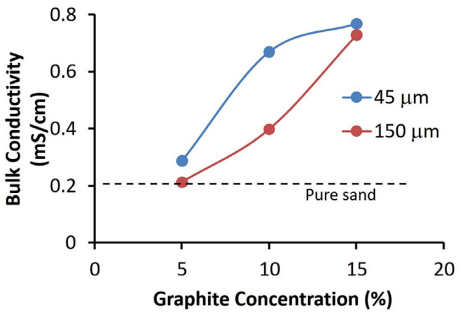

Figure 11. The effect of graphite concentrations on the bulk conductivity of the mixture at 10 mM NaCl pore fluid concentration.

Particle interconnection at higher concentrations

As can be noted from the spectral data (Fig. 4), increase the concentration of graphite particles in the mixture does not lead to a significant increase of the phase response at high frequencies. The change is rather small or even reversed. This is particularly evident in the case of 45 μm graphite particle mixtures at 10 per cent and 15 per cent concentrations (Fig. 4a). While high-frequency responses do not increase much or decreases significantly, the emergence of a low-frequency peak is observed in both cases with the two different particle sizes. This is, again, more evident in the case of 45um graphite particles (Fig. 4a). Additional evidences based on bulk conductivity data sets suggest that this is primarily due to the effects of particle interconnection or aggregation at 10 per cent and 15 per cent particle concentrations that increased the effective particle size and reduced the polarizable surface area of discrete fine particles. Fig. 12 shows that the bulk conductivity of the mixtures with 10 per cent and 15 per cent graphite is significantly higher than the pure sand at low frequency (1 Hz) under the same pore fluid (10 mM). Such an increase of the bulk conductivity is due to the formation of continuous, low resistance electronic pathways through the interconnected graphite particles that effectively increase the overall conductivity of the system. Such an effect has been observed in metallic particles, such as zero valent iron at similar concentrations (Slater *et al.* 2005). Fig. 11 also shows that even at only 5 per cent of graphite content, the bulk conductivity of the mixture is elevated for the 45 μm particles, which is an evidence of particle interconnection. This is not the case for the 150 μm graphite at 5 per cent concentration as its bulk conductivity is identical to that of the pure sand. This suggests a well dispersed graphite particle distribution in the sand matrix with little effect on bulk conductivity. As showed before, BET measurements indicate that the specific surface area of the 45 μm graphite is smaller than the 150 μm graphite. This suggests the likely presence of a more significant fraction of larger graphite particles in the 45 μm graphite, which may promote particle interconnection. It is also important to note that graphite particles have the tendency to form aggregates with further promotes particle interconnection, particularly when a large amount of particles is present. An overall increase of the relaxation time constant with increasing graphite concentration also supports the interconnection between graphite particle at high concentrations as shown in Fig. 12.

CONCLUSION

Graphite particles of different sizes and concentrations were studied for their SIP responses under different fluid salinity and pH conditions in this study. Significant enhancement of the SIP responses

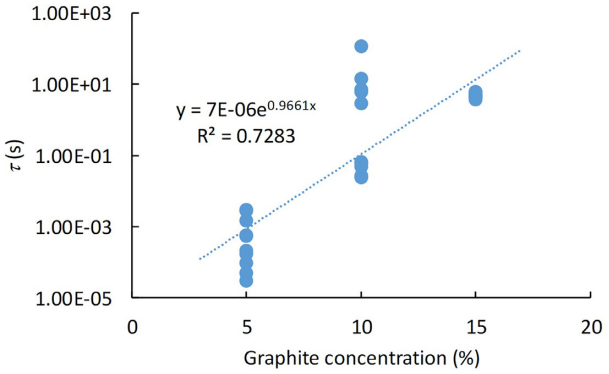

Figure 12. The correlation between graphite concentration and the relaxation time constant from the Cole–Cole model. The experimental results from the fluid conductivity experiments with both sizes of graphite particles are aggregated together in this plot.

is observed with graphite inclusion suggesting its large polarization responses when excited by an external electrical field. Our results suggest that pore water salinity has a strong impact on the phase and chargeability responses of graphite particles when the individual grains are well dispersed. While smaller in magnitude, the impact of pH on the magnitude of the phase and chargeability are notable and show consistent trends. The impacts of pore fluid salinity on the relaxation time constant agree with the existing literature. Such an impact is also observed when pH is systematically changes although the magnitude is smaller. Our experiments also suggest strong particle interconnection effects when higher concentrations of graphite are tested, for example, 10 and 15 per cent by volume. Such interconnection/aggregation effectively enlarges the polarizable particle size while reducing specific surface area of small particles. This has a significant impact on the magnitude and shape of the SIP spectrum with significant decrease of high-frequency phase signals, and concurrent emerging of larger phase responses at lower frequencies. These results suggest that while the volumetric concentration of graphite has a significant impact on its polarization signal, the geometrical arrangement of the particles in a mineral composite as well as the pore fluid chemistry, such as salinity and pH, are all major determining factors of graphite's polarization behaviour.

ACKNOWLEDGEMENTS

Funding for this research is provided by the U.S. Department of Energy, Office of Science, Office of Basic Energy Sciences, Chemical Sciences, Geosciences, and Biosciences Division, through its Geoscience program at LBNL under contract DE-AC02-05CH11231. YW designed and conducted the experiments, processed and analysed the data and wrote the paper. LP analysed the data, performed Cole–Cole model fitting and commented on the paper. We thank the Editor, Andréa Ustra, and an anonymous reviewer for their constructive comments that helped improve the manuscript.

REFERENCES

Bucker, M., Orozco, A.F. & Kemna, A., 2018. Electrochemical polarization around metallic particles—Part 1: the role of diffuse-layer and volume-diffusion relaxation, *Geophysics,* **83**(4), E203–E217.

Cole, K.S. & Cole, R.H., 1941. Dispersion and absorption in dielectrics. I: alternating current characteristics, *J. Chem. Phys.,* **9,** 341–351.

Gurin, G., Tarasov, A., Ilyin, Yu. & Titov, K., 2013. Time domain spectral induced polarization of disseminated electronic conductors: laboratory data analysis through the Debye decomposition approach, *J. Appl. Geophys.,* **98,** 44–53.

Gurin, G., Titov, K., Ilyin, Y. & Tarasov, A., 2015. Induced polarization of disseminated electronically conductive minerals: a semi-empirical model, *Geophys. J. Int.,* **200,** 1555–1565.

Kinchin, G.H., 1953. The electrical properties of graphite, *Proc. R. Soc. A,* **217,** doi:10.1098/rspa.1953.0043.

Klein, J.D. & Shuey, R.T., 1978. Nonlinear impedance of mineral–electrolyte interfaces: Part II. Galena, chalcopyrite, and graphite, *Geophysics,* **43**(6), 1235–1249.

Krishnan, K.S & Ganguli, N., 1939. Large anisotropy of the electrical conductivity of graphite, *Nature,* **144,** 667, doi:10.1038/144667a0.

Lesmes, D.P. & Frye, K.M., 2001. Influence of pore fluid chemistry on the complex conductivity and induced polarization responses of Berea sandstone, *J. geophys. Res.,* **106**(B3), 4079–4090.

Marshall, D.J. & Madden, T.R., 1959. Induced polarization, a study of its causes, *Geophysics,* **26,** 790–816.

Merriam, J., 2007. Induced polarization and surface electrochemistry, *Geophysics,* **72**(4), F157–F166.

Misra, S., Torres-Verdín, C., Revil, A., Rasmus, J. & Homan, D., 2016. Interfacial polarization of disseminated conductive minerals in absence of redox-active species. Part 1: mechanistic model and validation, *Geophysics,* **81**(2), E139–E157.

Pedraza, D.F & Klemens, P.G., 1993. Effective conductivity of polycrystalline graphite, *Carbon,* **31**(6), 951–956.

Pelton, W., Ward, S., Hallof, P., Sill, W. & Nelson, P.H., 1978, Mineral discrimination and removal of inductive coupling with multi-frequency IP, *Geophysics,* **43,** 588–609.

Peruzzo, L., Schmutz, M., Franceschi, M., Wu, Y. & Hubbard, S.S., 2018. The relative importance of saturated silica sand interfacial and pore fluid geochemistry on the spectral induced polarization response, *J. geophys. Res.,* **123,** 1702–1718.

Placencia-Gómez, E. & Slater, L.D., 2014. Electrochemical spectral induced polarization modeling of artificial sulfide-sand mixtures, *Geophysics,* **79**(6), EN91–EN106.

Revil, A., 2012. Spectral induced polarization of shaly sands: influence of the electrical double layer, *Water Resour. Res.,* **48,** W02517, doi:10.1029/2011WR011260.

Revil, A. & Skold, M., 2011. Salinity dependence of spectral induced polarization in sands and sandstones, *Geophys. J. Int.,* **187,** 813–824.

Revil, A., Florsch, N. & Mao, D., 2015. Induced polarization response of porous media with metallic particles—Part 1: a theory for disseminated semiconductors, *Geophysics,* **80**(5), D525–D538.

Revil, A., Mao, D., Shao, Z., Sleevi, M.F. & Wang, D., 2017. Induced polarization response of porous media with metallic particles—Part 6: the case of metals and semimetals, *Geophysics,* **82**(2), E97–E110.

Revil, A., Coperey, A., Mao, D., Abdulsamad, F., Ghorbani, A., Rossi, M. & Gasquet, D., 2018. Induced polarization response of porous media with metallic particles—Part 8: influence of temperature and salinity, *Geophysics,* **83,** E435–E456.

Skold, M., Revil, A. & Vaudelet, P., 2011. The pH dependence of spectral induced polarization of silica sands: experiment and modeling, *Geophys. Res. Lett.,* **38,** L12304, doi:10.1029/2011GL047748.

Slater, L. & Lesmes, D., 2002. Electrical-hydraulic relationships observed for unconsolidated sediments, *Water Resour. Res.,* **38**(10), 1213, doi:10.1029/2001WR001075.

Slater, L.D., Choi, J. & Wu, Y., 2005. Electrical properties of iron-sand columns: implications for induced polarization investigation and performance monitoring of iron-wall barriers, *Geophysics,* **70**(4), G87–G94.

Tarasov, A & Titov, K., 2013. On the use of the Cole–Cole equations in spectral induced polarization, *Geophys. J. Int.,* **195,** 352–356.

Ustra, A., Mendonca, C.A., Ntarlagiannis, D. & Slater, L.D., 2016. Relaxation time distribution obtained from a Debye decomposition of spectral induced polarization data, *Geophysics,* **81**(2), E129–E138.

Vinegar, H.J. & Waxman, M.H., 1984. Induced polarization of shaly sands, *Geophysics,* **49,** 1267–1287.

Wong, J., 1979. An electrochemical model of the induced-polarization phenomenon in disseminated sulfide ores, *Geophysics,* **44,** 1245–1265.